Ocean Sci., 6, 61–76, 2010
www.ocean-sci.net/6/61/2010/
© Author(s) 2010. This work is distributed under
the Creative Commons Attribution 3.0 License.

Ocean Science

Comparison of global ocean colour data records

S. Djavidnia[1,*], F. Mélin[1], and N. Hoepffner[1]

[1]European Commission – Joint Research Centre, Institute for Environment and Sustainability, TP272, via Fermi, 2749, 21027, Ispra, Italy
[*]now at: European Maritime Safety Agency, Cais do Sodré, 1249-206, Lisboa, Portugal

Received: 16 July 2009 – Published in Ocean Sci. Discuss.: 23 July 2009
Revised: 1 December 2009 – Accepted: 11 January 2010 – Published: 27 January 2010

Abstract. The extending record of ocean colour derived information, an important asset for the study of marine ecosystems and biogeochemistry, presently relies on individual satellite missions launched by several space agencies with differences in sensor design, calibration strategies and algorithms. In this study we present an extensive comparative analysis of standard products obtained from operational global ocean colour sensors (SeaWiFS, MERIS, MODIS-Aqua, MODIS-Terra), on both global and regional scales. The analysis is based on monthly mean chlorophyll *a* (Chl-*a*) sea surface concentration between 2002 and 2009.

Based on global statistics, the Chl-*a* records appear relatively consistent. The root mean square (RMS) difference Δ between (log-transformed) Chl-*a* from SeaWiFS and MODIS Aqua amounts to 0.137, with a bias of 0.074 (SeaWiFS Chl-*a* higher). The difference between these two products and MERIS Chl-*a* is approximately 0.15. Restricting the analysis to 2007 only, Δ between MODIS Aqua and Terra is 0.142. This global convergence is significantly modulated regionally. Statistics for biogeographic provinces representing a partition of the global ocean, show Δ values varying between 0.08 and 0.3. High latitude regions, as well as coastal and shelf provinces are generally the areas with the largest differences. Moreover, RMS differences and biases are modulated in time, with a coefficient of variation of Δ varying between 10% and 40%, with clear seasonal patterns in some provinces.

The comparison of the province-averaged time series obtained from the various satellite products also shows a level of agreement that is geographically variable. Overall, the Chl-*a* SeaWiFS and MODIS Aqua series appear to have similar levels of variance and display high correlation coefficients, an agreement likely favoured by the common elements shared by the two missions. These results are degraded if the MERIS series is compared to either SeaWiFS or MODIS Aqua. An important outcome of the study is that the results of the inter-comparison analysis are variable with time and location, and therefore globally averaged statistics are not necessarily applicable on a seasonal or regional basis.

Correspondence to: F. Mélin
(frederic.melin@jrc.ec.europa.eu)

1 Introduction

Satellite ocean colour has added another dimension to marine biology and ecosystem studies. The first satellite sensor devoted to the measurement of ocean colour was the NASA Coastal Zone Color Scanner (CZCS) launched in late 1978. In spite of being scheduled as a one-year demonstration program, the CZCS mission generated a large data set over the global ocean for more than seven years (Feldman et al., 1989), providing key information on the temporal and spatial distribution of phytoplankton and the magnitude of primary production at global scale (e.g., Yoder et al., 1993; Longhurst et al., 1995). Ultimately, it galvanized space agencies to prepare other ocean colour missions with more advanced sensors.

Consequently, over the last decade, several ocean colour space sensors have been launched for a regional or global coverage, providing unprecedented views of the marine systems with a better accuracy than CZCS owing to more advanced characteristics of the sensors themselves, but also to a substantial progress in the characterization of the instrument calibration and the performance of atmospheric correction and bio-optical models to support the signal processing. As a result, the applications of ocean colour imagery have considerably expanded, becoming a major component of marine biogeochemical and ecological programmes (IOCCG, 2008), and ocean colour is now listed as an Essential Climate

Variable originally identified in the Global Climate Observing System Implementation Plan (GCOS, 2006).

In order to construct a continuous time series of bio-optical and geophysical variables, the ocean colour community currently relies on a number of individual missions launched by several space agencies, with radiometric sensors from various manufacturers and with slightly different technical specifications. Variations in calibration strategies and algorithm formulations further amplify differences in the final satellite products that hamper the full exploitation of overlapping data sets. It has been long recognized that the task of creating a consistent ocean colour data stream from independent time series was particularly challenging (McClain, 1998), and required a complete set of assessments, from the analysis of the radiometric performance of the sensors (calibration, bias, instrumental artefact) during their operational lifetime (Evans and Gordon, 1994) to the quantification of the differences between sensor-specific products at the various processing levels (IOCCG, 2007). Preliminary global or regional inter-comparison exercises have already been conducted (e.g., Kwiatkowska, 2003; Djavidnia et al., 2006; Zhang et al., 2006; Mélin et al., 2009). These studies underlined significant differences between products, even though the broad patterns and general statistics usually appeared consistent. In order to reach more general and robust conclusions, it appears timely to take stock of the existing multi-annual satellite time series to assess the differences between their products in a systematic manner.

This work contributes to this effort by analysing differences between global records of concentration of chlorophyll-*a* (Chl-*a*). Four missions with a multi-annual global coverage are considered in this exercise, the Sea-viewing Wide Field-of-view Sensor (SeaWiFS, Hooker et al., 1992), the MEdium Resolution Imaging Spectrometer (MERIS, Rast et al., 1999), and the MODerate resolution Imaging Spectroradiometers (MODIS, Salomonson et al., 1989) on board the platforms Terra and Aqua. The analysis quantifies the differences between the monthly time series of Chl-*a* provided by these missions, with a focus on their seasonal and regional variability. Admittedly, using monthly composites for such an exercise integrates differences created by the irregular sampling associated with each sensor. Conversely, averaging pixel values over time in a given spatial bin reduces possible differences due to noise. As a matter of fact, monthly Chl-*a* time series are extensively used to study the regional to global algal seasonal variability (e.g., Carr and Kearns, 2003; Dandonneau et al., 2004), interannual anomalies (Murtuggude et al., 1999; Behrenfeld et al., 2001), relationships between biology and physics (Wilson and Coles, 2005), and long-term trends in the Chl-*a* record (Gregg et al., 2005; Vantrepotte and Mélin, 2009), or to validate outputs of biogeochemical models (e.g., Gregg et al., 2003; Vichi et al., 2007). Therefore it appears highly relevant to document the discrepancies associated with these Chl-*a* data sets.

The final aim of the work is to build a framework to monitor the Chl-*a* data records provided by the ocean colour missions. Its original developments have been established under the Marine Environment and Security for the European Area (MERSEA) project of the European Union. This effort is to be continued in the future, by regularly updating the statistical results as the ocean colour time series extends and by repeating the exercise after major reprocessing events.

2 Data and methods

This section presents the satellite products and the methods of analysis. It is underlined that these products are those directly distributed by space agencies to the user community.

2.1 Satellite data

2.1.1 Satellite missions

The main satellite products analysed in this work are the standard Chl-*a* fields associated with the SeaWiFS, MODIS-Aqua (i.e., MODIS on the Aqua platform) and MERIS missions. Additionally, the products from the MODIS-Terra mission are also included for a tentative evaluation. All four sensors are flying on polar orbiting platforms, collecting data at several wavelengths in the visible and near-infrared part of the electromagnetic spectrum, with equator crossing time between approximately 10:00 and 13:30.

The processing version associated with both SeaWiFS and MODIS corresponds to the SeaWiFS reprocessing 5.2 (July 2007), and the data are available from the Ocean Biology Processing Group (OBPG) at NASA's Goddard Space Flight Center (GSFC)[1]. The SeaWiFS products used in this analysis cover the time interval May 2002 to April 2009, but the data for January, February, March and July 2008 are excluded because of missing or insufficient coverage during these months. SeaWiFS products are available before these dates but with no overlap with the other missions included in the work. Considering the duration and quality of the record (McClain et al., 2004), the SeaWiFS data are selected as the reference set when appropriate. The products available for MODIS Aqua and Terra cover the period July 2002 to April 2009, and January 2007 to April 2009, respectively. Even though the Terra mission has been on orbit since December 1999, Level-3 products are currently distributed only for this limited interval.

MERIS flies on-board the ENVIronment SATellite (ENVISAT) from the European Space Agency (ESA). The products result from the second MERIS reprocessing (MEGS 7.4) and are available from the ESA Level-3 MERIS portal[2]. The series analysed here covers the period May 2002 to April 2009.

[1] http://oceancolor.gsfc.nasa.gov

[2] http://www.enviport.org/meris/lv3_main.htm

This study focuses on products with an on-going, and comparatively long time series. Other ocean colour missions have flown during the SeaWiFS period, including some with a global coverage, namely the POLarization and Directionality of the Earth's Reflectance 2 (POLDER-2) and the GLobal Imager sensor (GLI) (both on-board the Japanese Advanced Earth Observation Satellite II). Unfortunately, these missions were interrupted after nine months of coverage in 2003, and are not included in the present analysis.

2.1.2 Gridded products

The four satellite products considered here comply with a similar mapping scheme consistent with the recommendations of the IOCCG (2004). Pixel values are first accumulated into bins, the number of which decreases with the cosine of latitude in the zonal direction. The number of bins in the meridional direction is 2160 for MERIS and SeaWiFS, and 4320 for MODIS corresponding, respectively, to 4320 and 8640 bins in the zonal direction at the equator, and to spatial resolutions of 9.26 and 4.63 km, respectively. Monthly Chl-*a* distributions have been obtained by evaluating the mean of all available daily values over a month. Subsequently, these products have been re-mapped onto common rectangular grids with a number of grid points equal to 4320 and 2160 in longitude and latitude, respectively (i.e., a resolution of 1/12°).

2.1.3 Algorithms

The Chl-*a* products associated with the four sensors are derived following similar principles. The top-of-atmosphere radiance reflected by the Earth system is registered at several wavelengths in the visible to near-infrared (NIR) and interpreted for clear-sky conditions by atmospheric correction schemes. The NIR bands are essentially used to quantify the aerosol type and optical thickness in order to remove the contribution from the atmosphere in the visible part of the spectrum (Gordon and Wang, 1994; Antoine and Morel, 1999). For the considered processing chains, the result of the atmospheric correction is the normalized water-leaving radiance L_{WN}, obtained after correction for bi-directional effects (Morel et al., 2002). It is underlined here that the SeaWiFS and MODIS missions follow the same strategy in terms of calibration and atmospheric correction (Franz et al., 2007).

The spectrum of L_{WN} is then used to compute Chl-*a* with empirical maximum band-ratio algorithms created using simultaneous in situ data of Chl-*a* and marine optics. The principle of the algorithm is to express (in log-space) Chl-*a* as a 4th-degree polynomial expression of the maximum of band ratios between 2 or 3 bands in the blue part of the spectrum and one green band. The ratios are between remote sensing reflectance (for SeaWiFS and MODIS) or irradiance reflectance (for MERIS).

The algorithm used to evaluate the SeaWiFS Chl-*a* is OC4v4 (O'Reilly et al., 2000), with band ratios combining remote sensing reflectance at 443, 490, or 510 nm with the green band (555 nm). The algorithm for MODIS, OC3M, is constructed with the same ensemble of field observations, but uses only two channels in the blue (443 and 488 nm) with respect to a green band at 551 nm. Similarly to SeaWiFS, MERIS Chl-*a* (CHL 1 product, Morel and Antoine, 2007) is based on a four-band algorithm with the channels at 442, 490, 510 nm (blue bands) and 560 nm (green band). It is important to point out that these algorithms assume a direct relationship between band ratios and Chl-*a*, in the general context of Case 1 waters (Morel and Maritorena, 2001), and it is recognized that their application to coastal waters, where other optically significant constituents affect the apparent optical properties, is likely to be associated with high uncertainties.

2.2 Methods

Statistics are expressed as a function of the logarithm (base 10) of Chl-*a*, assuming a log-normal distribution as the most appropriate statistical representation of the data. This is documented in previous works (Campbell, 1995; Gregg and Casey, 2004), and is further supported in the present analysis by computing statistics of skewness and kurtosis for global fields of multi-annual Chl-*a* averages that are illustrated on Fig. 1. For the log-transformed distribution of Chl-*a*, skewness and kurtosis are typically equal to 1 and 3, respectively, whereas these indicators are respectively one and two orders of magnitude higher for untransformed Chl-*a*.

The analysis focuses on monthly products. As acknowledged in the Introduction, differences in times of overpass and sampling over the month are likely to generate part of the differences between monthly gridded composites. On the other hand, averaging pixel values in space (into grid points) and over time reduces the scattering due to noise. For any two satellite products and for each month, the pairs of coincident valid Chl-*a* values are identified and stored. Considering a given period and/or region (ensemble of grid points, province or global ocean), these pairs can be pooled into an ensemble for comparison. Chl-*a* values are weighted by the surface associated with each grid point. In practice, the magnitude of the difference between the Chl-*a* distributions with N common elements associated with two sensors 1 and 2 is expressed by the root mean square (RMS) difference (Δ) and bias (δ), computed in $\log_{10}$ space (Gregg and Casey, 2004):

$$\Delta = \left(\frac{1}{N}\sum_{i=1}^{N}[\log(\mathrm{Chl}_{2,i}) - \log(\mathrm{Chl}_{1,i})]^2\right)^{1/2} \quad (1)$$

$$\delta = \frac{1}{N}\sum_{i=1}^{N}[\log(\mathrm{Chl}_{2,i}) - \log(\mathrm{Chl}_{1,i})] \quad (2)$$

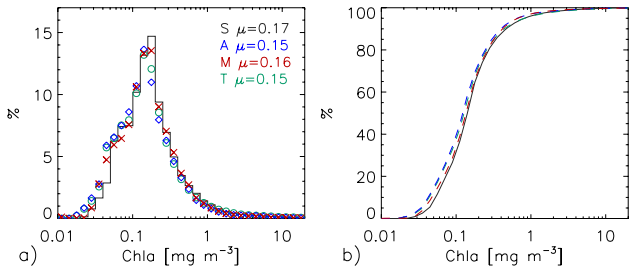

Fig. 1. **(a)** Frequency distribution and **(b)** cumulative frequency distribution of multi-annual Chl-*a* (with histogram bins of 0.1 in logarithm of Chl-*a*). The geometric average μ of the distribution (in mg m^{-3}) is given for each sensor product, indicated by its reference letter (S for SeaWiFS, A for MODIS Aqua, M for MERIS, and T for MODIS Terra). The different sensors are identified by specific colors and symbols: for (a) black line for SeaWiFS, blue diamonds for MODIS-Aqua, red crosses for MERIS, and green circles for MODIS-Terra, and for (b) black line for SeaWiFS and coloured dashed lines for the other products.

These indicators are accompanied by the unbiased root mean square (URMS) difference (Δ_u):

$$\Delta_u = \left(\frac{1}{N} \sum_{i=1}^{N} [(\log(\mathrm{Chl}_{2,i}) - \overline{\mathrm{LC}_2}) - (\log(\mathrm{Chl}_{1,i}) - \overline{\mathrm{LC}_1})]^2 \right)^{1/2} \quad (3)$$

where $\overline{\mathrm{LC}_k}$ indicate the average of the distributions $(\log(\mathrm{Chl}_{k,i}))_{i=1,N}$ for the sensor k.

The comparison results are evaluated in terms of both global spatial distribution and specific oceanic regions. To derive global maps of statistical indicators for a given time frame (typically the entire series or a specific season), calculations are made on the ensemble of pairs of valid Chl-*a* values found in this time frame. For instance, maps of statistics for boreal winter are constructed by pooling all valid pairs identified for the months of December, January or February (DJF) found in the common satellite series. A similar analysis is made for spring (March, April, May, MAM), summer (June, July, August, JJA), and autumn (September, October, November, SON), and for a multi-year annual average (all months). In the latter case, calculations are based on complete years only to avoid introducing a bias due to a possible seasonal dependence of the statistics. So, multi-annual statistics are based on the intervals January 2003 to December 2007 for the comparison between SeaWiFS and MODIS-Aqua or MERIS, January 2003 to December 2008, for the comparison between MODIS-Aqua and MERIS, and January to December 2007 for the comparison between the MODIS on Aqua and Terra (see below for a discussion on Terra). To increase the statistical basis of the calculations, valid pairs are also aggregated in space for subsets of 4×4 grid points, so that statistics are shown on maps with a resolution of a 1/3° (but it is underlined that the matching pairs are still identified at the 1/12° resolution). These maps have been compared with similar maps with no spatial aggregation, and show similar patterns and amplitudes but with a lower level of noise (not shown). Finally, statistics are not displayed if based on less than 10% of the maximum number of valid pairs. This number corresponds to the number of months included in the time frame (for instance 60 for 5-year multi-annual statistics) multiplied by the aggregation factor (4×4 here). The arbitrary threshold of 10% is chosen to allow a large spatial coverage of the results (see Sect. 3.2) while excluding grid points where statistics rely on a small number of months. Changing the threshold affects only the spatial extent of the displayed result. With a threshold of 10%, the percentage of marine grid points with statistics constructed with an insufficient number of months (essentially in high-latitude regions) is 7%, 9%, 10% and 6% for the comparison between SeaWiFS and MODIS-Aqua, SeaWiFS and MERIS, MERIS and MODIS-Aqua, and MODIS Aqua and Terra, respectively. This percentage increases to 12%, 16%, 17% and 12% if the threshold is raised to 20%.

The second focus of the analysis is on regional scales. The global ocean is partitioned into the biogeographic provinces proposed by Longhurst (1998) (Fig. 2) with minor modifications (separate provinces for Baltic and Black Seas). The complete description of these provinces and the associated patterns of Chl-*a* temporal variability, as well as the definition of acronyms, can be found in Longhurst (1998) and Vantrepotte and Mélin (2009). For a given month and province (or set of provinces), the pairs of coincident valid Chl-*a* values are selected to compute the statistical indicators. Final indicators representative of each province are then derived by computing the multi-annual average (and standard deviation) on the same set of complete years mentioned above. Moreover, the series of Chl-*a* averaged on every province have also been derived for each mission using the same procedure. To get robust statistics, the calculations are not performed if the comparison ensemble covers less than an arbitrary threshold of 10% of the province surface. A change in this threshold does not overly affect the results. For instance, raising it to 20% decreases the number of valid months with comparison statistics for 16 to 20 provinces (considering only the three main pairs of sensors), located mostly at high latitudes. This decrease in the number of valid months is on average 4.2 (on a potential maximum of 60 or 70), with a change in the value of the average Δ for the affected provinces averaging 0.003.

3 Global statistics

In the description of the results, the satellite missions are referred to as *S*, *A*, *T* and *M* for SeaWiFS, MODIS-Aqua, MODIS-Terra and MERIS, respectively. Thus, Chl-a_S indicates Chl-*a* for SeaWiFS, $\Delta(A{:}S)$ refers to the term Δ computed between the distributions Chl-a_S and Chl-a_A, and $\delta(A-S)$ refers to the term δ computed for the difference Chl-a_A–Chl-a_S. In the analysis related to MODIS Terra, for

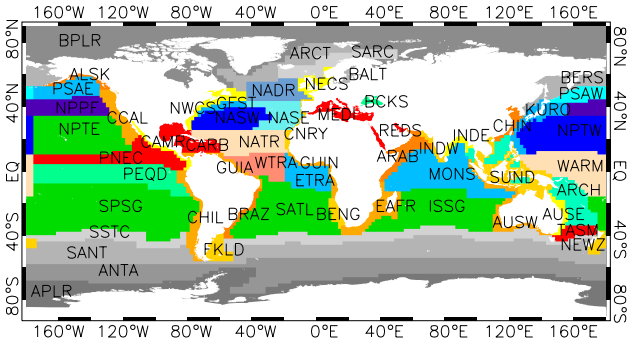

Fig. 2. Definition of the provinces used for statistical analyses.

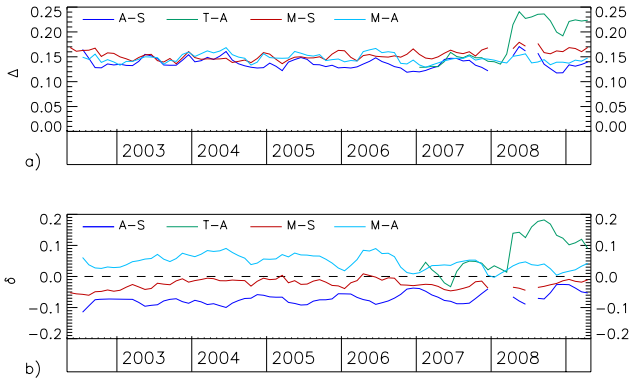

Fig. 3. Time series of **(a)** Δ and **(b)** δ computed at global scale.

the sake of simplicity only the pair with the two MODIS instruments, (A:T), is considered. Seasons are referred to by the acronyms introduced above (i.e., DJF, MAM, JJA and SON).

3.1 General results

The frequency distributions of the multi-annual global field of Chl-*a* are shown on Fig. 1. The multi-annual global distribution is here computed independently for each sensor on a common period, January 2003 to December 2007 (except for MODIS Terra, 2007 only), to allow a direct comparison. The four frequency distributions appear remarkably similar across the entire range of Chl-*a*, with overall geometric averages in the interval 0.15–0.17 mg m^{-3} (with the values for MODIS-Aqua and SeaWiFS the lowest and largest, respectively). Subtle variations can however be noticed. MODIS Aqua and Terra Chl-*a* distributions are slightly shifted toward lower values (as clearly seen on the cumulative frequency distributions, Fig. 1b), whereas the proportion of Chl-*a* values in the interval 0.15–0.40 mg m^{-3} is higher for SeaWiFS and MERIS.

Figure 3 shows the time series of the RMS difference (Δ) and bias (δ) computed at global scale. An important result is that these statistical indicators vary little in time. Thus, Δ is found in the interval 0.12–0.18 for the three pairs (S:A), (S:M) and (A:M). The terms δ are slightly more variable, in the interval -0.12 to $+0.09$ for the same three pairs (Fig. 3b). In 2007, $\Delta(T{:}A)$ and $\delta(T-A)$ are consistent with the other terms, but increases in 2008. Considering that the global average Chl-*a* from Terra also increases concurrently and abruptly (not shown), whereas the Chl-*a* record from Aqua (as well as that from SeaWiFS and MERIS) is fairly constant, this behaviour is likely associated with uncorrected variations in the calibration of Terra (Franz et al., 2008), and justifies the choice of computing statistics for MODIS Terra using only data of 2007. With the exception of MODIS Terra, no significant drift in the Chl-*a* records is revealed by the comparison, and an analysis based on seasonal and multi-annual averages appear to give representative results for the period.

Average global statistics are given in Table 1 (first line). The RMS difference between Chl-a_S and Chl-a_A is 0.137($\pm$0.010) and is only slightly higher for the pairs with MERIS (0.147–0.150). The coefficient of variation (CV) of Δ (ratio of standard deviation and average) varies between 5% and 7%, confirming the stability of Δ over time. The Chl-a_S and Chl-a_M records are separated by a low bias, -0.021 on average (Fig. 3 and Table 1). The level of Chl-a_A appears lowest, generating biases $\delta(A-S)$ of -0.074 and $\delta(M-A)$ of +0.049. For the pair (T:A), $\Delta(T{:}A)$ and $\delta(T-A)$ are 0.142 and +0.022, respectively.

3.2 Global spatial and seasonal variability

The global distribution of the RMS difference (Δ) and bias (δ) in Chl-*a* is shown in Figs. 4 (overall average of Δ) and 5 (seasonal averages for δ). Over a large part of the world ocean, the differences between each pair of sensor-specific products remain reasonably low with Δ values ranging between 0.03 and 0.15. On the other hand, higher Δ values, with multi-annual averages that may exceed 0.25, can be observed systematically at specific locations, particularly at high latitudes and in coastal and shelf regions, such as the Guinea (GUIN) and Guianas (GUIA) coastal provinces or the upwelling systems along the west coast of Africa or America. In the tropical Atlantic, increased cloud cover and complex aerosol mixtures often observed in this region (Quinn et al., 2001) provide challenging conditions for the ocean colour algorithms and may additionally restrict the data availability for the comparative analysis, which in turn can amplify the differences between sensor products. Likewise, conditions encountered in high latitude regions might be particularly critical for ocean colour remote sensing because of low sun zenith angles and possible adjacency effects from bright snow-covered (ice and land) surfaces and sub-pixel contamination by sea ice (Bélanger et al., 2007). Moreover, the scarcity of data may also contribute to the high Δ values in spring and summer. The map displaying $\Delta(A{:}T)$ (Fig. 3d) is fairly consistent with the other comparisons, but with fairly

Table 1. Statistics of comparison for the globe and each province. See Fig. 2 for location. Statistics are computed on log-transformed Chl-*a* distributions. The temporal average (± standard deviation) are given. In the case of Δ, the coefficient of variation (ratio of standard deviation and average) is given in brackets in %. Horizontal lines arbitrarily classify provinces as belonging to Atlantic, Indian, Pacific and Southern Oceans.

	A-S		M-S		M-A	
	Δ	δ	Δ	δ	Δ	δ
GLOB	0.14±0.01 (7%)	−0.07±0.01	0.15±0.01 (5%)	−0.02±0.01	0.15±0.01 (6%)	0.05±0.02
BPLR	0.23±0.05 (21%)	−0.13± 0.04	0.28±0.05 (16%)	−0.13±0.05	0.21±0.03 (15%)	0.00±0.04
ARCT	0.17±0.04 (21%)	−0.08± 0.02	0.21±0.04 (19%)	−0.04±0.08	0.18±0.05 (26%)	0.04±0.07
SARC	0.19±0.04 (19%)	−0.10± 0.03	0.23±0.04 (19%)	−0.07±0.08	0.18±0.04 (22%)	0.03±0.07
NADR	0.14±0.02 (17%)	−0.06±0.02	0.18±0.03 (18%)	0.01±0.05	0.17±0.04 (26%)	0.06±0.05
GFST	0.13±0.04 (29%)	−0.05±0.02	0.16±0.04 (28%)	−0.00±0.05	0.16±0.04 (25%)	0.05±0.04
NASW	0.11±0.01 (13%)	−0.07±0.02	0.14±0.04 (32%)	−0.03±0.06	0.13±0.03 (27%)	0.04±0.05
NATR	0.16±0.05 (33%)	−0.12±0.05	0.15±0.05 (31%)	−0.05±0.04	0.16±0.04 (29%)	0.06±0.03
WTRA	0.17±0.02 (13%)	−0.11±0.02	0.14±0.02 (15%)	−0.02± 0.03	0.17±0.03 (18%)	0.09±0.03
ETRA	0.17±0.03 (18%)	−0.11±0.02	0.17±0.03 (19%)	−0.05± 0.04	0.17±0.03 (18%)	0.06±0.04
SATL	0.12±0.02 (13%)	−0.08±0.02	0.13±0.03 (26%)	−0.03±0.04	0.13±0.02 (19%)	0.05±0.05
NECS	0.15±0.03 (17%)	−0.08±0.03	0.21±0.05 (22%)	−0.07±0.07	0.19±0.04 (23%)	0.01±0.06
CNRY	0.21±0.03 (16%)	−0.04±0.04	0.24±0.03 (14%)	−0.05±0.06	0.29±0.05 (16%)	−0.00±0.08
GUIN	0.28±0.05 (18%)	−0.10±0.03	0.31±0.06 (21%)	−0.09±0.06	0.30±0.06 (21%)	0.03±0.07
GUIA	0.23±0.04 (16%)	−0.09±0.02	0.24±0.04 (15%)	−0.05±0.03	0.26±0.04 (17%)	0.04±0.03
NWCS	0.14±0.03 (23%)	−0.06±0.03	0.18±0.04 (22%)	−0.03±0.05	0.17±0.03 (20%)	0.03±0.04
MEDI	0.09±0.02 (17%)	−0.06±0.02	0.12±0.02 (17%)	0.01±0.05	0.12±0.03 (20%)	0.06±0.05
CARB	0.14±0.04 (27%)	−0.08±0.03	0.14±0.03 (18%)	−0.02±0.03	0.16±0.03 (20%)	0.06±0.03
NASE	0.11±0.01 (12%)	−0.06±0.02	0.14±0.03 (18%)	−0.02±0.03	0.13±0.04 (29%)	0.06±0.04
BRAZ	0.14±0.02 (17%)	−0.06±0.02	0.18±0.03 (18%)	−0.04±0.03	0.18±0.03 (18%)	0.01±0.04
FKLD	0.14±0.03 (20%)	−0.04±0.04	0.19±0.06 (33%)	−0.03±0.06	0.21±0.06 (28%)	−0.00±0.07
BENG	0.14±0.02 (15%)	−0.04±0.02	0.20±0.03 (13%)	−0.06±0.04	0.22±0.02 (11%)	−0.03±0.03
BCKS	0.11±0.04 (36%)	−0.05±0.04	0.17±0.06 (33%)	−0.05±0.08	0.16±0.05 (30%)	0.01±0.06
BALT	0.21±0.05 (26%)	0.02±0.06	0.30±0.08 (28%)	−0.19±0.08	0.34±0.09 (28%)	−0.22±0.11
MONS	0.12±0.02 (14%)	−0.06± 0.02	0.11±0.02 (15%)	0.01±0.02	0.13±0.02 (18%)	0.07±0.02
ISSG	0.13± 0.02 (13%)	−0.09± 0.02	0.13±0.04 (30%)	−0.03±0.05	0.13±0.02 (18%)	0.06±0.05
EAFR	0.12± 0.01 (12%)	−0.07± 0.02	0.14±0.02 (15%)	−0.02±0.02	0.14±0.02 (14%)	0.05±0.02
REDS	0.14± 0.02 (12%)	−0.09± 0.02	0.14±0.02 (16%)	0.01±0.05	0.18±0.04 (21%)	0.09±0.06
ARAB	0.17± 0.06 (33%)	−0.06± 0.04	0.16±0.05 (34%)	−0.03±0.03	0.20±0.06 (30%)	0.04±0.06
INDE	0.17± 0.06 (36%)	−0.09± 0.03	0.19±0.07 (38%)	−0.00±0.05	0.21±0.08 (37%)	0.09±0.07
INDW	0.19± 0.08 (42%)	−0.07± 0.04	0.19±0.07 (39%)	−0.01±0.05	0.23±0.09 (38%)	0.06±0.07
AUSW	0.11± 0.01 (13%)	−0.05± 0.01	0.14±0.02 (13%)	0.01±0.03	0.14±0.01 (10%)	0.05±0.02
BERS	0.18± 0.04 (22%)	−0.10± 0.03	0.24±0.08 (32%)	−0.09±0.09	0.19±0.06 (31%)	0.01±0.08
PSAE	0.13± 0.03 (27%)	−0.05± 0.03	0.17±0.04 (26%)	−0.01±0.07	0.16±0.04 (25%)	0.04±0.07
PSAW	0.15± 0.03 (24%)	−0.06± 0.03	0.20±0.06 (29%)	−0.03±0.07	0.18±0.06 (32%)	0.03±0.07
KURO	0.15± 0.02 (16%)	−0.07± 0.02	0.17±0.03 (18%)	−0.03±0.04	0.16±0.03 (20%)	0.04±0.04
NPPF	0.11± 0.02 (22%)	−0.05± 0.02	0.15±0.04 (24%)	0.01±0.05	0.15±0.03 (23%)	0.05±0.04
NPTW	0.14± 0.02 (17%)	−0.09± 0.03	0.14±0.03 (18%)	−0.04±0.03	0.12±0.02 (17%)	0.04±0.04
TASM	0.10± 0.02 (20%)	−0.05± 0.02	0.12±0.02 (21%)	−0.01±0.04	0.12±0.02 (18%)	0.04±0.04
SPSG	0.15± 0.02 (12%)	−0.10± 0.02	0.14±0.03 (21%)	−0.03±0.04	0.13±0.02 (12%)	0.06±0.05
NPTE	0.13± 0.02 (19%)	−0.09± 0.03	0.15±0.03 (24%)	−0.05±0.05	0.13±0.02 (20%)	0.04±0.04
PNEC	0.12± 0.01 (10%)	−0.07± 0.02	0.13±0.02 (20%)	−0.01±0.02	0.13±0.02 (15%)	0.06±0.03
PEQD	0.08± 0.01 (15%)	−0.05± 0.01	0.08±0.01 (17%)	0.01±0.02	0.09±0.01 (15%)	0.05±0.02
WARM	0.14± 0.02 (12%)	−0.04± 0.02	0.15±0.02 (14%)	0.02±0.03	0.14±0.02 (13%)	0.06±0.03
ARCH	0.13± 0.01 (8%)	−0.07± 0.01	0.14±0.02 (14%)	0.01±0.02	0.14±0.01 (9%)	0.07±0.03
ALSK	0.18± 0.05 (26%)	−0.09± 0.03	0.24±0.07 (29%)	−0.09±0.09	0.21±0.05 (26%)	0.00±0.08
CCAL	0.11± 0.01 (13%)	−0.04± 0.02	0.16±0.03 (20%)	−0.00±0.04	0.16±0.04 (27%)	0.03±0.04
CAMR	0.15± 0.03 (19%)	−0.04± 0.02	0.18±0.03 (16%)	−0.01±0.03	0.18±0.03 (19%)	0.03±0.03
CHIL	0.17± 0.01 (8%)	−0.05± 0.02	0.20±0.03 (13%)	−0.06±0.03	0.20±0.03 (14%)	−0.01±0.03
CHIN	0.16± 0.03 (18%)	−0.06± 0.02	0.22±0.05 (23%)	−0.06±0.06	0.22±0.05 (21%)	0.02±0.05
SUND	0.15± 0.02 (10%)	−0.05± 0.01	0.18±0.02 (11%)	0.02±0.03	0.18±0.02 (9%)	0.07±0.02
AUSE	0.13± 0.02 (14%)	−0.07± 0.02	0.16±0.02 (13%)	−0.03±0.04	0.16±0.02 (10%)	0.04±0.03
NEWZ	0.11± 0.02 (19%)	−0.04± 0.02	0.15±0.02 (16%)	−0.01±0.04	0.15±0.03 (17%)	0.03±0.04
SSTC	0.12± 0.02 (20%)	−0.07± 0.03	0.13±0.02 (15%)	−0.01±0.04	0.14±0.02 (12%)	0.05±0.04
SANT	0.13± 0.02 (18%)	−0.07± 0.03	0.16±0.02 (15%)	−0.03±0.04	0.16±0.02 (13%)	0.04±0.03
ANTA	0.13± 0.02 (11%)	−0.05± 0.02	0.23±0.05 (22%)	−0.07±0.05	0.21±0.04 (20%)	−0.02±0.05
APLR	0.19± 0.02 (12%)	−0.06± 0.01	0.27±0.03 (12%)	−0.09±0.05	0.25±0.03 (11%)	−0.04±0.05

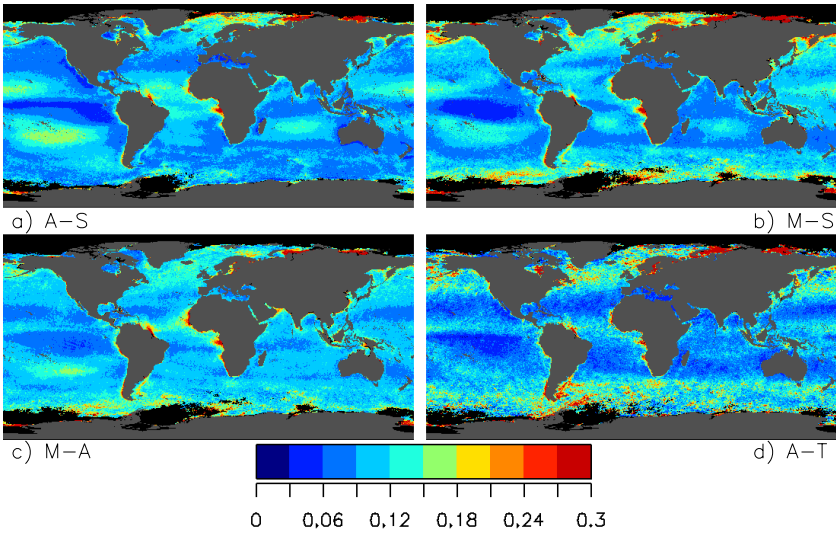

Fig. 4. Spatial distribution (1/3°) of the multi-annual average of Δ obtained for the satellite pairs **(a)** (S:A), **(b)** (S:M), **(c)** (A:M), and **(d)** (A:T).

high differences in the Southern Ocean. The spatial distribution of $\Delta(A{:}T)$ also appears noisy, probably due to the shorter data availability associated with MODIS-Terra. Thus, the seasonal variations of $\delta(T-A)$ are not shown in Fig. 5. In terms of multi-annual values, the global distribution of $\delta(T-A)$ is mostly slightly positive (not shown).

Interestingly, fairly large differences between sensor products also occur periodically in the middle of the oceanic gyres. These differences appear substantial between MODIS-Aqua and SeaWiFS in both the north and south Pacific, and the north Atlantic gyres, particularly during the seasons MAM and JJA, whereas a similar level of differences only persists in the south Pacific gyre during DJF and SON. These patterns are found in association with large negative biases (Fig. 5, left-hand column). In all cases, MODIS-Aqua would tend to significantly underestimate Chl-*a* in these oligotrophic environments when compared with SeaWiFS. Actually, the regions with positive seasonal averages for $\delta(A-S)$ are very few (e.g., Patagonian shelf or western equatorial Pacific in DJF). In general, the maps of δ involving MERIS are more heterogeneous than those shown for $\delta(A-S)$. In the same way as for the (S:A) comparison, MERIS is inclined to underestimate Chl-*a* compared to SeaWiFS in regions where large differences Δ are observed between both sensor products, e.g., at sub-tropical latitudes (south in DJF, north in MAM and JJA), in the Southern Ocean in DJF and in the Northern Hemisphere high latitudes during JJA. Outside these areas, the bias $\delta(M-S)$ becomes positive, particularly along the equator and at temperate latitudes. Consistent with a general positive bias (Fig. 3), the difference $\delta(M-A)$ is positive over most of the global ocean (Fig. 5, right-hand column), except in specific regions such as Pacific and Atlantic sub-tropical latitudes (south in DJF, north in JJA) or the Arabian Sea (in DJF). $\delta(M-A)$ is particularly high in austral winter (JJA) in the whole Southern Hemisphere.

4 Regional results

The examination of Figs. 4 and 5 reveals that, besides clear seasonal variations, the spatial distributions of RMS differences and biases exhibit patterns that can be associated with specific oceanographic provinces, warranting a regional analysis that is hereby structured by the major ocean basins and the provinces displayed on Fig. 2. The statistics resulting from this analysis are given in Table 1 as multi-annual averages and standard deviations for each province. It is recalled that the calculations have been performed on a set of complete years. The multi-annual statistics are displayed for all provinces on Figs. 6 to 8 in the form of Δ_u versus δ plots, also called target diagram (Jolliff et al., 2009). These diagrams are efficient to summarize information about differences by plotting unbiased RMS (the component of the total RMS difference not due to the bias) and bias, as well as the total RMS Δ that is the distance from the point of origin (as determined by the relation $\Delta^2{=}\delta^2{+}\Delta_u^2$). On each plot, the global average is also reported (note that the scales vary for each figure).

4.1 Arctic and Southern Ocean provinces

The Baltic (BALT) and Bering Seas (BERS) are arbitrarily pooled with the Arctic provinces (ARCT, SARC). As already anticipated from the analysis of the maps, Arctic and Southern Ocean provinces tend to be characterized by differences higher than the global average (Figs. 6a to 8a). This is particularly true for the Arctic provinces and for the

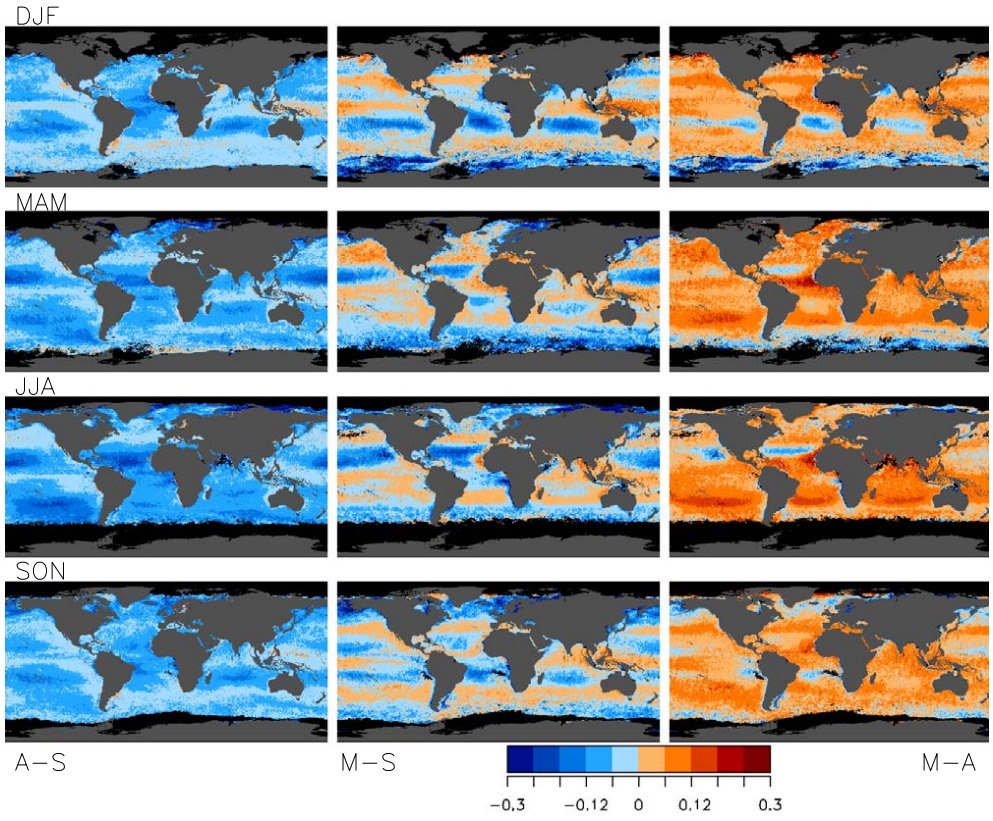

Fig. 5. Spatial distribution (1/3°) of the multi-annual seasonal averages of δ obtained for the satellite pairs $A-S$ (left-hand column)), $M-S$ (centre column), and $M-A$ (right-hand column). From top to bottom, the four seasons are DJF (December, January, February), MAM (March, April, May), JJA (June, July, August), and SON (September, October, November).

pairs (S:A) and (S:M). In general, the Baltic Sea (BALT) and the Boreal Polar province (BPLR) are characterized by large differences, with Δ exceeding 0.2 or 0.3. Considering the three pairs of comparison, BALT is the province with the highest levels of Δ, and is the only province with $\delta(A-S)$ positive (+0.02, Table 1). For the pairs (S:M) and (A:M), Δ for BALT is increased by a large bias (approximately 0.2, actually the largest value among provinces). Besides its high latitudes, the Baltic Sea is characterized by a strong contribution to absorption from chromophoric dissolved organic matter (CDOM). Not surprisingly, standard bio-optical algorithms have been shown to produce large discrepancies with field data (Darecki and Stramski, 2004). Moreover, the satellite products derived from band ratios are likely to be quite noisy because of the low values usually observed for L_{WN} as well as intense and heterogeneous events like cyanobacteria blooms (e.g., Zibordi et al., 2006; Kutser, 2004). These conditions certainly tend to increase the discrepancies found between the satellite records. Interestingly, the Bering Sea shows a clear seasonality in Δ for the pairs (S:M) and (A:M), with values peaking in spring and exceeding 0.3. The provinces of the Southern Ocean (APLR, ANTA, SANT, SSTC and NEWZ) have lower levels of differences with respect to the Arctic, and show a decreasing gradient of Δ from the Antarctic provinces (APLR, ANTA, Δ greater than 0.19, except for (S:A) in ANTA) northward to sub-antarctic waters. In Arctic and Southern Ocean waters, cloud cover and sea ice are factors likely increasing the differences between the satellite records. It is also worth noting that large discrepancies between satellite and field values have been documented for these regions. Large biases have been shown to contribute significantly to these differences (Cota et al., 2004; Gregg and Casey, 2004; Korb et al., 2004), even though this has been questioned for the Southern Ocean (Marrari et al., 2006).

4.2 Atlantic Ocean

The statistics obtained for the Atlantic Ocean show a rather large spread (Figs. 6b to 8b). Overall, the two coastal provinces GUIA and GUIN, and the Benguela and Canary upwelling regions (BENG and CNRY) are the provinces with the largest differences, with Δ exceeding 0.2 for all pairs (except $\Delta(S$:$A)$ for BENG, equal to 0.14). In fact, GUIN is the province with the highest Δ of all provinces for the three pairs considered. As already mentioned, the tropical

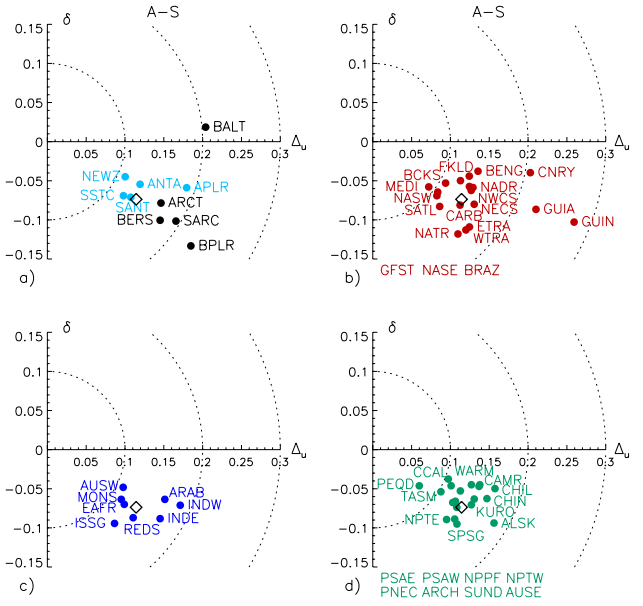

Fig. 6. Target diagram for the pair $(A - S)$ (MODIS-Aqua versus SeaWiFS), plotting bias δ versus unbiased RMS difference Δ_u, computed for each province and averaged over 2003–2007. The provinces are displayed per basin: **(a)** Arctic and Southern Ocean provinces (black and light blue, respectively), **(b)** Atlantic Ocean, **(c)** Indian Ocean, and **(d)** Pacific Ocean. The dashed circles are isolines of equal RMS difference Δ. The globally averaged statistics are indicated by a black diamond. To avoid cluttering, some province acronyms (close to the global average) are listed below the diagram.

Atlantic is characterized by challenging atmospheric conditions in terms of cloud cover and aerosols. Dust transport from northwest Africa is a conspicuous feature (Kaufman et al., 2005) and can also impact southwest Africa (Eckardt and Kuring, 2005), and biomass burning seasonally affects equatorial and southern Africa with absorbing aerosols (e.g., Haywood et al., 2003). Besides these atmospheric conditions, the upwelling centres are characterized by dynamic features such as filaments (e.g., Gabric et al., 1993) that might introduce variability between large scale monthly satellite products. On the other side of the basin, the South American river outflows impact a large area of the tropical Atlantic with waters having optical properties departing from conditions typical of the open ocean (Hu et al., 2004). Otherwise, the statistics for the other provinces tend to be constrained in a rather small interval around the global average. For the pair $(S{:}A)$, they vary in the range 0.11–0.17, with the highest values (0.16–0.17) for the equatorial Atlantic provinces (NATR, WTRA and ETRA), a result associated with large bias values ($\delta(A-S)$ of -0.11 to -0.12, Fig. 6b). For the pairs $(S{:}M)$ and $(A{:}M)$, Δ is mainly found in the interval 0.13–0.18, with some higher values associated with coastal/shelf provinces, namely $\Delta(S{:}M)$ equal to 0.19 for FLKD and 0.21 for NECS, $\Delta(A{:}M)$ equal to 0.19 for NECS and 0.21 for FKLD. In the case of the $(A{:}M)$ pair, the bias is clearly higher for the large open ocean provinces than for coastal/shelf ones (+0.04 to +0.09 versus -0.0 to +0.04).

Two marginal seas have been included in this section, the Mediterranean (MEDI) and Black (BCKS) Seas. For the three pairs considered, Δ associated with MEDI is among the three lowest of all provinces, as low as 0.09 for $(S{:}A)$. This convergence is fairly consistent with the high correlation observed between satellite derived Chl-*a* and field data over a background of large biases (Bricaud et al., 2002; Volpe et al., 2007; Mélin et al., 2007). For the pair $(S{:}A)$, Δ for the Black Sea is also among the lowest of all provinces (0.11), whereas it is slightly higher than the global average when MERIS is involved (0.16–0.17). These rather small differences are in fact remarkable; indeed, the Black Sea is characterized by a significant degree of uncertainty for the standard ocean colour products (Sancak et al., 2005; Oguz and Ediger, 2006), meso- and sub-mesoscale structures (like filaments and meanders) in the ocean colour signal (Oguz et al., 2002), and extreme and heterogeneous events like large-scale blooms of coccolithophores (Cokacar et al., 2004), elements that could increase the differences between independent satellite records.

4.3 Indian Ocean

The eight Indian Ocean provinces (Fig. 2) present statistics mostly spread between the Δ isolines 0.1 to 0.2 (Figs. 6c to 8c). In the case of the pairs $(S{:}A)$ and $(S{:}M)$, all Δ values are below 0.2. The three provinces of the northern Indian Ocean coasts and shelf (ARAB, INDW, INDE) are characterized by the highest Δ for the three pairs of sensors (around 0.2 for the pair $(A{:}M)$). The northern Indian Ocean is certainly very challenging for ocean colour remote sensing, particularly from the atmospheric point of view, oscillating between two circulation regimes, the southwest monsoon in summer with aerosols dominated by sea salt and dust (Vinoj and Satheesh, 2003) and the northeast winter monsoon heavily influenced by absorbing anthropogenic and continental (including desert) aerosols from the Indian sub-continent (Ramanathan et al., 2001). The RMS difference for the other provinces is usually lower than, or equal to, the global average. The bias $\delta(A - S)$ varies between -0.05 and -0.09 (for the southern gyre ISSG), and $\delta(M - A)$ between +0.04 (ARAB) and +0.09 (REDS and INDE). In the case of $(S : M)$, the bias is remarkably small for all provinces ($\delta(M - S)$ between -0.03 and +0.01).

4.4 Pacific Ocean

The statistics of the Pacific provinces appear mostly clustered around the global averages (Figs. 6d to 8d). For the three satellite pairs, the provinces ALSK (Alaska coastal province), CHIL (Chile/Peru upwelling) and CHIN (Chinese

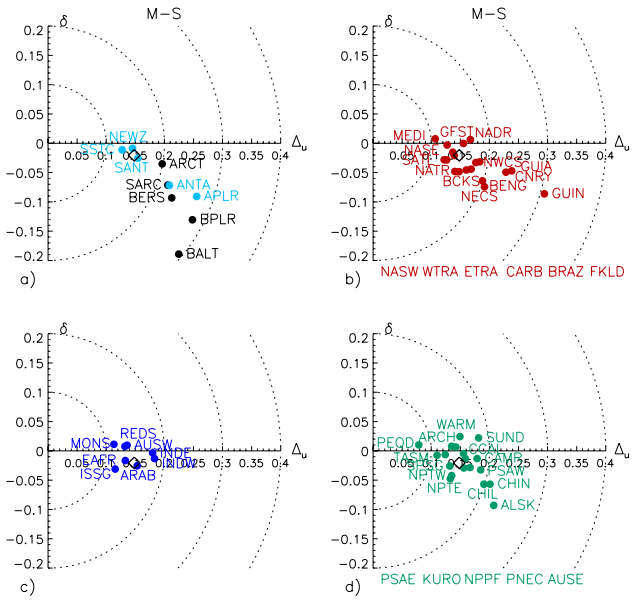

Fig. 7. Same as Fig. 6, for the pair $(M-S)$ (MERIS versus SeaWiFS).

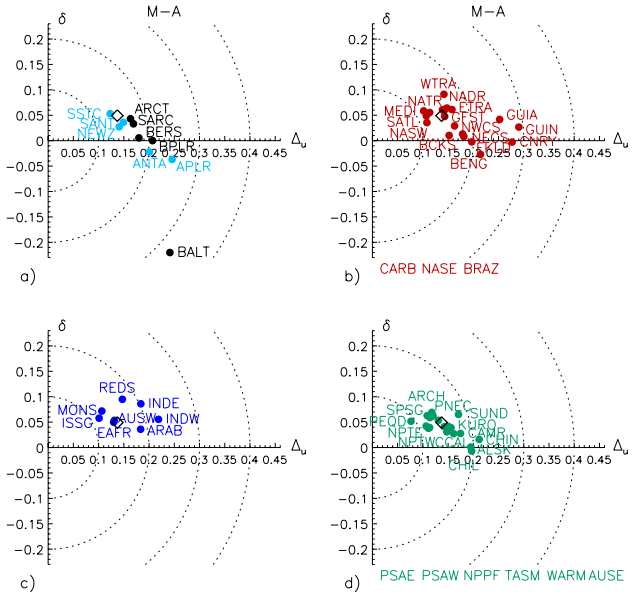

Fig. 8. Same as Fig. 6, for the pair $(M-A)$ (MERIS versus MODIS-Aqua), for the period 2003–2008.

seas) show the highest levels of Δ (exceeding 0.2 for the pairs $(S{:}M)$ and $(A{:}M)$). Zhang et al. (2006) have compared full-resolution SeaWiFS and MODIS-Aqua Chl-*a* products for the South China Sea and Taiwan Strait and have obtained RMS differences of approximately 0.13 over one year, which is lower than for the whole CHIN statistics presented here (0.16). Differences are also fairly high for the North Pacific provinces (PSAW, PSAE, KURO), particularly for the pairs involving MERIS. At the other end, the equatorial Pacific province PEQD shows the lowest values of Δ of all provinces (0.08–0.09). This may be put in the context of low differences observed between field measurements and SeaWiFS Chl-*a* products in the equatorial Pacific (RMS differences of 0.17, Gregg and Casey, 2004). For the pair $(S{:}A)$, the bias $\delta(A-S)$ varies between −0.04 and −0.10 (for the southern Pacific gyre, SPSG). Excluding the three provinces with high Δ (ALSK, CHIL and CHIN), $\delta(M-S)$ is in the interval −0.05 (NPTE) to +0.02 (Pacific "warm pool", WARM), and $\delta(M-A)$ in the interval +0.03 to +0.07 (ARCH and SUND).

4.5 Cross-basin comparison

Except for the Arctic Ocean, the basins taken as a whole show similar values of statistical indicators. For instance, $\Delta(S{:}A)$ is found equal to 0.13–0.14 for the four oceans (Atlantic, Pacific, Indian and Southern). For $(S{:}M)$ and $(A{:}M)$, the range is 0.13–0.16 and 0.14–0.16, respectively. However, some differences emerge if the provinces are classified into broad categories. Gyre and tropical provinces are characterized by Δ values below average (less than 0.14 for all three satellite pairs), whereas it is slightly higher for mid-latitude waters. In the equatorial band, it is worth underlining that differences are significantly higher in the Atlantic (provinces WTRA and ETRA) than in the Pacific and Indian oceans. Thus, Δ is found equal to 0.17, 0.15 and 0.17 in the Atlantic for the pairs $(S{:}A)$, $(S{:}M)$ and $(A{:}M)$, respectively, whereas it is 0.11, 0.12 and 0.12 in the equatorial Pacific (grouping the provinces PEQD, PNEC and WARM). The larger discrepancies in the tropical Atlantic have been mentioned previously (Fig. 4). Differences for coastal/shelf provinces and the four major upwelling regions (BENG, CCAL, CHIL, CNRY) are higher than the global averages, particularly for the satellite pairs involving MERIS. For shelf/coastal areas, Δ is equal to 0.16, 0.19 and 0.19 for the pairs $(S{:}A)$, $(S{:}M)$ and $(A{:}M)$, respectively, and 0.15, 0.19 and 0.20 for the upwelling ensemble.

In view of the European focus of the MERSEA project, it is worth underlining the variety of comparison statistics for European seas, that reflects their diversity in terms of optical types (Berthon et al., 2008). In general, as coastal/shelf regions and marginal seas, they tend to be characterized by differences larger than the global average (Table 1). This is particularly the case for the northern regions (provinces BALT and SARC), and the Canary upwelling area (CNRY), and to a lesser extent for the northwest Atlantic shelf (NECS). As indicated in Sect. 4.2, the Black Sea have levels of Δ slightly lower (for the pair $(S{:}A)$) and higher (for $(S{:}M)$ and $(A{:}M)$) than the global average, and the Mediterranean Sea is a basin with a remarkable convergence between the various products.

4.6 Temporal variability of the differences

Table 1 lists the average and standard deviation of Δ over the course of multi-year time series, together with the coefficient of variation (CV, which is the ratio between the two values), that may serve as an indicator of the temporal variability of Δ. For all three satellite pairs, CV is found between approximately 10% and 40%. The pairs involving MERIS are associated with a higher level of variations, with 26 and 29 provinces for (S:M) and (A:M), respectively, having CV larger than 20%. For the pair (S:A), a CV greater than 20% is found in 19 provinces.

The temporal variability of Δ and δ varies among the provinces, and it is difficult to find general rules. Some provinces, with a rather low CV, show fairly constant values of these statistical indicators. The largest of these areas is the tropical Pacific and Indo-Pacific region (PEQD, WARM, ARCH, SUND). In turn, these cases correspond to weak variations of the Chl-*a* signal itself. Conversely, some regions display short-term variability of the differences, typically in regional/shelf seas such as the Black Sea, the Arabian Sea, the Red Sea/Persian Gulf (REDS), the Chinese shelf (CHIN) or the Canary upwelling (CNRY). Finally, a clear seasonal cycle for Δ and/or δ is evident for some regions. For instance, in the Gulf Stream province (GSFT), Δ tends to be higher (lower) in boreal spring (autumn) corresponding with the maxima (minima) of Chl-*a*. The case of the North Atlantic tropical gyre province (NATR) is interesting: Δ for the three sensor pairs varies with the season between approximately 0.1 in boreal winter and 0.25 in summer whereas the Chl-*a* average signals show very little variability; moreover, only $\delta(A-S)$ and $\delta(M-S)$ show a clear seasonal signal (more negative in summer). Still in the Atlantic, only $\delta(M-S)$ and $\delta(M-A)$ associated with the southern gyre SATL show a clear seasonal variability, with lower values in austral summer (more negative for (S:M) and closer to 0 for (A:M)) corresponding to the Chl-*a* seasonal minimum. Further to this it is interesting to observe that similar patterns are also seen for the Indian and Pacific counterparts, the southern gyre provinces ISSG and SPSG. Other provinces exhibit a distinct signal in Δ, e.g., GUIA, the Caribbean Sea (CARB), the Indian coastal provinces (INDW and INDE), the California Current province (CCAL), or the Bering Sea (BERS).

4.7 RMS differences and biases

Considering the bias existing between the different satellite products, as shown along the y-axis of the target diagrams (Figs. 6 to 8), it is worth assessing how much the systematic differences between the data sets contribute to the RMS difference. Two experiments have been performed to investigate this aspect. First, for each satellite pair, one satellite data set is systematically corrected by the global bias, enabling a globally unbiased comparison. The average Δ for the pair (S:A) decreases from 0.137 to 0.114; the decrease is less for $\Delta(S{:}M)$, from 0.150 to 0.149, and for $\Delta(A{:}M)$, from 0.147 to 0.138. For the pair (S:M), the small gain in Δ is partly explained by the small original bias ($\delta(M{:}S)$ of -0.02). A second experiment is conducted with a bias correction applied to each province separately. The RMS difference Δ is then 0.112 for (S:A), 0.147 for (S:M), and 0.136 for (A:M). So, only in the case of the pair (S:A) is a reduction of the overall bias translated into a significant reduction of the global average of the RMS difference, whereas introducing a bias correction with regional variations does not largely improve the global statistics.

5 Comparison of temporal variability

The previous sections have focused on statistics based on ensembles of coincident pairs of Chl-*a* values. Another approach is to compare the Chl-*a* records obtained independently by each mission for representative regions of the ocean, in other words to assess how these Chl-*a* records are consistent in magnitude and phase. This is indeed a typical exercise performed between biogeochemical model outputs and satellite data. The approach is first presented and the results are illustrated thereafter.

5.1 Analysis of the time series

The approach followed to assess the differences between the Chl-*a* records pictured by the various satellite missions is based on Taylor diagrams (Taylor, 2001), as these provide a useful mean to summarize pattern statistics between two ensembles of values (e.g., Mélin et al., 2007; Friedrichs et al., 2009). Here, the SeaWiFS time series is considered as the reference data set for comparison with the MODIS-Aqua and MERIS counterparts. The series of reference is represented on the x-axis of the 2-D diagram by its standard deviation σ_r; the series to be compared is represented by a point situated at a radial distance from the origin equal to the standard deviation of this series, σ, the cosine of the angle between this radial and the x-axis being the correlation coefficient r between the two series. By construction the unbiased RMS difference Δ_u is then the distance between the two points. The position of the points simultaneously illustrates the following elements: (i) the level of correlation between the two series; (ii) a comparison of their respective standard deviations, and; (iii) the unbiased RMS differences (Figs. 9 to 10).

These statistics have been computed for specific provinces or groups of provinces that are representative cases and actually encompass much of the global ocean. To allow an easy interpretation between regions, the standard deviations have been normalized to the SeaWiFS value, so that the SeaWiFS points converge to the value of 1 on the abscissa. The distance to that point is then the unbiased RMS difference normalized to the σ_r of each region, Δ'_u. In practice, the closer a point is located with respect to the abscissa, the more the

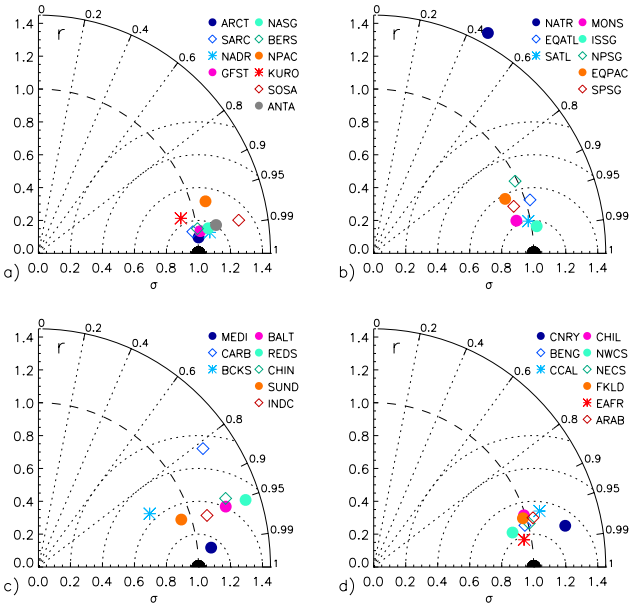

Fig. 9. Taylor diagrams, comparing the Chl-*a* records obtained for representative provinces or aggregations of provinces from SeaWiFS and MODIS-Aqua. The scale of the axes is the standard deviation normalized to that of the SeaWiFS Chl-*a* series. The SeaWiFS record is taken as a reference and associated with the black filled half circle on the abscissa. Coloured symbols indicate the comparison with the MODIS series. The quarter circle is scaled by the correlation coefficient. Dotted circles are isolines of equal normalized unbiased RMS differences. Dotted lines are lines of equal correlation. The four diagrams correspond to **(a)** high and mid latitude regions, **(b)** sub-tropical and equatorial provinces, **(c)** marginal seas, and **(d)** coastal, shelf and upwelling areas. See text for definition of some acronyms.

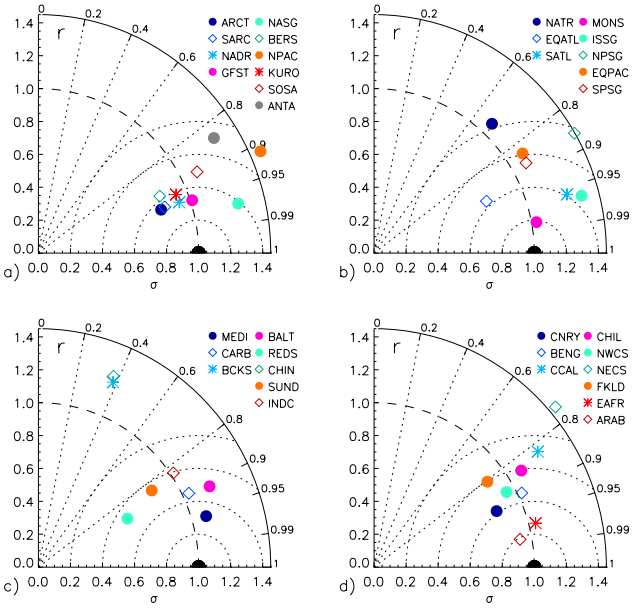

Fig. 10. Same as Fig. 9 for the pair SeaWiFS/MERIS.

series is correlated with that of SeaWiFS, and the standard deviation represented by that series is higher than the SeaWiFS value if the point is beyond the circle of radius 1.

5.2 Results

The four groups displayed on Figs. 9 and 10 are representative of: (i) mid to high latitude regions, (ii) equatorial and sub-tropical provinces, (iii) marginal seas, and (iv) upwelling, coastal and shelf regions. Some points are associated with aggregates of provinces, namely North Atlantic subtropical gyres (NASG: NASW and NASE), North Pacific (NPAC: PSAW, PSAE, NPPF, ALSK), Southern Ocean subantarctic waters (SOSA: SSTC and SANT), equatorial Atlantic (EQATL: WTRA and ETRA), North Pacific subtropical gyres (NPSG: NPTW and NPTE), equatorial Pacific (EQPAC: WARM, PNEC and PEQD), and Indian coastal waters (INDC: INDW and INDE). Even though this classification may be considered somewhat arbitrary, it nevertheless serves the purpose of the current discussion.

For the comparison between the SeaWiFS and MODIS-Aqua Chl-*a* records, most of the series are found with a correlation coefficient larger than 0.9 or even 0.95, and comparable standard deviations (points close to the circle of radius 1). This is particularly true for the mid to high latitude regions as well as the coastal areas (Fig. 9a and d). However, it is observed that the MODIS-Aqua Chl-a_A series for the subantarctic waters (SOSA) and the Canary upwelling (CNRY) are associated with a standard deviation higher than for SeaWiFS (at least 20% more). Most of the points are also characterized by a normalized RMS difference Δ'_u below 0.3. For subtropical and equatorial regions, the correlation tends to be lower (and Δ'_u higher, Fig. 9b). In this case, the province NATR appears as an outlier: the Chl-a_A series has a high σ with respect to SeaWiFS and the two signals are poorly correlated (r equal to 0.47). This might be due to the challenges facing ocean colour remote sensing in this region, as well as the low levels of seasonal variations found for Chl-*a*. Finally, there is an expected diversity in the results obtained for the marginal seas (Fig. 9c). The Chl-a_A series reproduce a relatively low σ in the Black Sea, and relatively high σ for the Red Sea/Persian Gulf (REDS), the Chinese shelf (CHIN), the Caribbean (CARB) and Baltic (BALT) Seas. On the contrary, the point associated with the Mediterranean Sea is very close to the reference point with r equal to 0.994.

In general, the comparison between the SeaWiFS and MERIS records show more scattered results (Fig. 10), with lower values for r and higher values for Δ'_u. A similar conclusion is reached if the MERIS and MODIS-Aqua series are compared (not shown). Once again, for the groups associated with the mid to high latitude regions and the coastal areas (Fig. 10a and d), the levels of standard deviation reproduced

by the MERIS Chl-a_M series are similar to the SeaWiFS series, the North Pacific (NPAC), North Atlantic subtropical gyres (NASG), the Antarctic province (ANTA), and the Northwest European shelf (NECS) being notable exceptions, with a higher σ for MERIS by a factor of at least 1.3. For the other groups, the points are more spread. For subtropical and equatorial provinces (Fig. 10b), Δ'_u is at least 0.4, except for the equatorial Indian Ocean (MONS). The equatorial and northern subtropical Pacific (EQPAC and NPSG) are associated with r of approximately 0.85, whereas r is as low as 0.68 for NATR. For the marginal seas (Fig. 10c), only the Mediterranean Sea has a Δ'_u lower than 0.4 (with r equal to 0.96). Otherwise, r is close to or below 0.9, and as low as 0.4 for the Black Sea and Chinese shelf (with the standard deviation reproduced by MERIS higher than that of Chl-a_S by a factor 1.2). Conversely, for the Red Sea/Persian Gulf, the standard deviation for Chl-a_M is only 0.63 times that of Chl-a_S.

6 Conclusions and discussion

The first major conclusion of this work is that the large scale (1/12°) monthly Chl-*a* time series produced by the three major multi-annual global ocean colour missions (SeaWiFS, MODIS-Aqua and MERIS) are relatively consistent, with average RMS differences (in log space) of 0.137 for the pair SeaWiFS/MODIS-Aqua, and approximately 0.15 between these sensors and MERIS. These differences are to be considered in the context of RMS differences between the daily Chl-*a* (SeaWiFS) product and field observations of 0.31 (Gregg and Casey, 2004). The global Chl-*a* frequency distributions provided by the three products are also remarkably alike (Fig. 1). Moreover, there is a satisfactory agreement with the MODIS-Terra series for 2007, whereas the use of this product for subsequent years is presently not recommended.

However, this global convergence appears significantly modulated on a regional basis. Using a partition of the global ocean into biogeographic provinces (Longhurst, 1998), the multi-annual averages of RMS difference vary between 0.08 and approximately 0.3. High latitude regions, and coastal/shelf provinces are generally the areas with the largest differences. Local maxima in Δ are also seen in the middle of some subtropical gyres (Fig. 4). Moreover, RMS differences and biases are also modulated in time, with a coefficient of variation varying between approximately 10% and 40%, and with clear seasonal patterns in some provinces. Particularly, a seasonal signal for the biases between MERIS and either SeaWiFS or MODIS-Aqua for the large southern subtropical gyres has been noticed. These regions do not display a strong seasonal cycle in Chl-*a* or aerosol type and load, so that differences in water type or atmospheric conditions are unlikely to fully explain the variations in bias. This seasonal signal in the bias terms might otherwise indicate a sensitivity of the final product to the geometry of illumination. Indeed, the seasonal cycle of solar illumination is to be considered as a possible explanatory factor because it systematically modulates the conditions encountered by the atmospheric correction schemes, and possibly their outputs. In any case, it is important to underline that multi-annual and globally averaged statistics provide only a very incomplete description of the difference between the Chl-*a* records.

An additional analysis has been performed by considering the province-averaged time series of Chl-*a* products as independent records. This type of exercise would typically be performed between satellite products and outputs of biogeochemical models (Jolliff et al., 2009). This analysis again underlines that the level of agreement between the series is very variable geographically. Overall, the SeaWiFS and MODIS-Aqua Chl-*a* series appear to have similar levels of variance and display high correlation coefficients. These results are degraded if the MERIS series is compared to either SeaWiFS or MODIS-Aqua. In general, the better convergence between the SeaWiFS and MODIS-Aqua records with respect to MERIS is likely favoured by the common processing elements shared by these two missions, but it might also indicate a higher level of uncertainty for the MERIS Chl-*a* product.

The exercise of satellite product inter-comparison answers several purposes. Differences and, even more importantly, biases have to be carefully investigated to address the creation of a long term seamless data record that is based on subsequent, partly overlapping, satellite missions. The space and time distribution of these statistics has to be taken into account in the data merging activities that are now being developed (Kwiatkowska and Fargion, 2003; Maritorena and Siegel, 2005; Pottier al., 2006; Mélin and Zibordi, 2007), and is required by data assimilation schemes (e.g., Gregg, 2008). The inter-comparison also provides a general insight into the levels of uncertainties that can be expected for the ocean colour record as a whole. For instance, the regions with large differences and/or biases between sensor products, are areas where uncertainties are likely to be high, or at least where the independent satellite records should be handled with more caution. Clearly the comparative analysis is not a substitute for an actual validation with field measurements. On the other hand, the statistics obtained by inter-comparison are available at global scale and for all seasons, a comprehensive character that validation exercises can not attain. The two types of exercises are thus complementary.

Investigating the factors responsible for the differences existing between the satellite products goes beyond the scope of the present work. The data records derived from the ocean colour missions are different for a variety of reasons, including the differences in instruments and calibration, different sets of bands and spatial resolutions, independent atmospheric correction schemes with specific aerosol models, corrections for white caps and sun glint, flagging sequences, and varying overpass times. Among these elements, characterizing the uncertainties and biases related

to the atmospheric correction for representative water types, and how these propagate through associated bio-optical algorithms (e.g., Mélin et al., 2005; Salama and Stein, 2009), seems critical. Some progress is forthcoming with the collection of more radiometric data at sea and the development of networks of autonomous instruments for the validation of satellite derived aerosol optical thickness and L_{WN} (Bailey and Werdell, 2006; Zibordi et al., 2009; Mélin et al., 2010). Differences in the outputs of the atmospheric correction schemes, combined with different bio-optical models and spatio-temporal mismatches, translate into further discrepancies between the sensor specific end-products considered here, the Chl-*a* concentration. It can be noticed that differences due to inconsistent algorithm formulations could be satisfactorily addressed (Morel et al., 2007). Ideally, the reduction of differences between end-products needs to rely on an integrated and cross-mission approach tackling all the mission components. A first step could be to aim at the reduction of the overall biases, thus acting to decrease the RMS differences (as quantified in Sect. 4.7), whereas errors associated with noise and environmental variability can be quantified with appropriate statistical approaches (with a global median estimated as 0.074 in log-scale for SeaWiFS and MODIS-Aqua Chl-*a* distributions, Mélin, 2010). This would facilitate the creation of a long term consistent data record and simplify the efforts of data merging and assimilation.

Acknowledgements. The authors thank the Ocean Biology Processing Group of NASA for the distribution of the SeaWiFS and MODIS products, and ESA for the MERIS products. This work has been partly funded by the Marine Environment and Security for the European Area (MERSEA) project of the European Union (contract AIP3-CT-2003-502885, 6th Framework Programme). The continuation of this activity is supported by the MyOcean project (No. 218812, EU 7th Framework Programme).

Edited by: L. Bertino

References

Antoine, D. and Morel, A.: A multiple scattering algorithm for atmospheric correction of remotely sensed ocean colour (MERIS instrument): Principle and implementation for atmospheres carrying various aerosols including absorbing ones, Int. J. Remote Sens., 20, 1875–1916, 1999.

Bailey, S. W. and Werdell, P. J.: A multi-sensor approach for the on-orbit validation of ocean color satellite data products, Remote Sens. Environ., 102, 12–23, 2006.

Behrenfeld, M. J., Randerson, J. T., McClain, C. R., Feldman, G. C., Los, S. O., Tucker, C. J., Falkowski, P. G., Field, C. B., Frouin, R., Esaias, W. E., Kolber, D. D., and Pollack, N. H.: Biospheric primary production during an ENSO transition, Science, 291, 2594–2597, 2001.

Bélanger, S., Ehn, J. K., and Babin, M.: Impact of sea ice on the retrieval of water-leaving reflectance, chlorophyll *a* concentration and inherent optical properties from satellite ocean color data, Remote Sens. Environ., 111, 51–68, 2007.

Berthon, J.-F., Mélin, F., and Zibordi, G.: Ocean colour remote sensing of the optically complex European seas, in: Remote Sensing of the European Seas, edited by: Barale, V. and Gade, M., Springer, 35–52, 2008.

Bricaud, A., Bosc, E., and Antoine, D.: Algal biomass and sea surface temperature in the Mediterranean basin. Intercomparison of data from various satellite sensors, and implications for primary production estimates, Remote Sens. Environ., 81, 163–178, 2002.

Campbell, J. W.: The lognormal distribution as a model for bio-optical variability in the sea, J. Geophys. Res., 100, 13237–13254, 1995.

Carr, M.-E. and Kearns, E. J.: Production regimes in four eastern boundary current systems, Deep-Sea Res. II, 50, 3199–3221, 2003.

Cokacar, T., Oguz, T., and Kubilay, N.: Satellite-detected early summer coccolithophore blooms and their interannual variability in the Black Sea, Deep-Sea Res. I, 51, 1017–1031, 2004.

Cota, G. F., Wang, J., and Comiso, J. C.: Transformation of global satellite chlorophyll retrievals with a regionally tuned algorithm, Remote Sens. Environ., 90, 373–377, 2004.

Dandonneau, Y., Deschamps, P.-Y., Nicolas, J.-M., Loisel, H., Blanchot, J., Montel, Y., Thieuleux, F., and Bécu, G.: Seasonal and interannual variability of ocean color and composition of phytoplankton communities in the North Atlantic, equatorial Pacific and South Pacific, Deep-Sea Res. II, 51, 303–318, 2004.

Darecki, M. and Stramski, D.: An evaluation of MODIS and SeaWiFS bio-optical algorithms in the Baltic Sea, Remote Sens. Environ., 89, 326–350, 2004.

Djavidnia, S., Mélin, F., and Hoepffner, N.: Assessment of global and regional ocean sea surface chlorophyll *a*, in: European Operational Oceanography: Present and Future, Proceedings of the 4th Conference on EuroGOOS, 2005, 122–127, 2006.

Eckardt, F. D. and Kuring, N.: SeaWiFS identifies dust sources in the Namib desert, Int. J. Remote Sens., 26, 4159–4167, 2005.

Evans, R. H and Gordon, H. R.: Coastal Zone Color Scanner system calibration: a retrospective examination, J. Geophys. Res., 99, 7293–7307, 1994.

Feldman, G. C., Kuring, N. A., Ng, C., Esaias, W. E., McClain, C. R., Elrod, J. A., Maynard, N., Endres, D., Evans, R., Brown, J., Walsh, S., Carle, M., and Podesta, G.: Ocean color: Availability of the global data set, EOS Trans. of the American Geophysical Union, 70, 634–641, 1989.

Franz, B. A., Bailey, S. W., Werdell, P. J., and McClain, C. R.: Sensor-independent approach to the vicarious calibration of satellite ocean color radiometry, Appl. Optics, 46, 5068–5082, 2007.

Franz, B. A., Kwiatkowska, E., Meister, G., and McClain, C. R.: Moderate Resolution Spectroradiometer on Terra: Limitations for ocean color applications, J. Appl. Remote Sens., 2, 023525, doi:10.1117/1.2957964, 2008.

Friedrichs, M. A. M., Carr, M.-E., Barber, R. T., Scardi, M., Antoine, A., Armstrong, R. A., Asanuma, I., Behrenfeld, M. J., Buitenhuis, E. T., Chai, F., Christian, J. R., Ciotti, A. M., Doney, S. C., Dowell, M., Dunne, J., Gentili, B., Gregg, W., Hoepffner, N., Ishizaka, J., Kameda, T., Lima, I., Marra, J., Mélin,, F., Moore, J. K., Morel, A., O'Malley, R. T., O'Reilly, J., Saba, V. S., Schmeltz, M., Smyth, T. J., Tjiputra, J., Waters, K., Westberry, T. K., and Winguth, A.: Assessing the uncertainties of model es-

timates of primary productivity in the tropical Pacific Ocean, J. Mar. Syst., 76, 113–133, 2009.

Gabric, A. J., Garcia, L., Van Camp, L., Nykjaer, L., Eifler, W., and Schrimpf, W.: Offshore export production in the Cape Blanc (Mauritania) giant filament as derived from Coastal Zone Color Scanner imagery, J. Geophys. Res., 98, 4697–4712, 1993.

GCOS, Report GCOS-107: Systematic observation requirements for satellite-based products for climate, in: Implementation Plan for the Global Observing System for Climate in Support of the UNFCCC - Supplemental details to the satellite-based component, WMO/TD No. 1338, 103 pp., 2006.

Gordon, H. R. and Wang, M.: Retrieval of water-leaving radiance and aerosol optical thickness over the oceans with SeaWiFS: a preliminary algorithm, Appl. Optics, 33, 443–452, 1994.

Gregg, W. W., Ginoux, P., Schopf, P. S., and Casey, N. W.: Phytoplankton and iron: Validation of a global three-dimensional ocean biogeochemical model, Deep-Sea Res. II, 50, 3143–3169, 2003.

Gregg, W. W. and Casey, N. W. : Global and regional evaluation of the SeaWiFS chlorophyll data set, Remote Sens. Environ., 93, 463–479, 2004.

Gregg, W. W., Casey, N. W., and McClain, C. R.: Recent trends in global ocean chlorophyll, Geophys. Res. Lett., 32, L03606, doi:10.1029/2004GL021808, 2005.

Gregg, W. W.: Assimilation of SeaWiFS ocean chlorophyll data into a three-dimensional global ocean model, J. Mar. Syst., 69, 205–225, 2008.

Haywood, J. M., Osborne, S. R., Francis, P. N., Keil, A., Formenti, P., Andreae, M. O., and Kaye, P. H.: The mean physical and optical properties of regional haze dominated by biomass burning aerosol measured from the C-130 aircraft during SAFARI 2000, J. Geophys. Res., 108, 8473, doi:10.1029/2002JD002226, 2003.

Hooker, S. B., Esaias, W. E., Feldman, G. C., Gregg, W. W., and McClain, C. R.: An overview of SeaWiFS and ocean color, NASA Technical Memorandum, 1992-104566, vol. 1, edited by: Hooker, S. B. and Firestone, E. R., NASA-GSFC, Greenbelt, Maryland, 1–24, 1992.

Hu, C., Montgomery, E. T., Schmitt, R. W., and Muller-Karger, F. E.: The dispersal of the Amazon and Orinoco River water in the tropical Atlantic and Caribbean Sea: Observation from space and S-PALACE floats, Deep-Sea Res. II, 51, 1151–1171, 2004.

IOCCG, 2004: Guide to the creation and use of ocean colour, Level-3, binned data products, Antoine D. (ed.), Campbell, J. W., Evans, R. H., Gregg, W. W., Lewis, M. R., Morel, A., Moulin, C., and Murakami, H., Report of the International Ocean Colour Coordinating Group no. 4, 88 pp., IOCCG, Dartmouth, Canada, 2004.

IOCCG, 2007: Ocean-Colour Data Merging, Gregg, W. W. (ed.), Aiken, J., Kwiatkowska, E., Maritorena, S., Mélin, F., Murakami, H., Pinnock, S., and Pottier, C., Report of the International Ocean Colour Coordinating Group, no.6, 68pp., IOCCG, Dartmouth, Canada, 2007.

IOCCG, 2008: Why ocean colour? The societal benefits of ocean colour technology, edited by: Platt, T., Hoepffner, N., Stuart, V., and Brown, C. W., Report of the International Ocean Colour Coordinating Group, no. 7, 141 pp., IOCCG, Dartmouth, Canada, 2008.

Jolliff, J. K., Kindle, J. C., Shulman, I., Penta, B., Friedrichs, M. A. M., Helber, R., and Arnone, R. A.: Summary diagrams for coupled hydrodynamic-ecosystem model skill assessment, J. Mar. Syst., 76, 64–82, 2009.

Kaufman, Y. J., Koren, I., Remer, L. A., Tanré, D., Ginoux, P., and Fan, S.: Dust transport and deposition observed from the Terra-Moderate Resolution Imaging Spectroradiometer (MODIS) spacecraft over the Atlantic Ocean, J. Geophys. Res., 110, D10S12, doi:10.1029/2003JD004436, 2005.

Korb, R. E., Whitehouse, M. J., and Ward, P.: SeaWiFS in the Southern Ocean: Spatial and temporal variability in phytoplankton biomass around South Georgia, Deep-Sea Res. II, 51, 99–116, 2004.

Kutser, T.: Quantitative detection of chlorophyll in cyanobacterial blooms by satellite remote sensing, Limnol. Oceanogr., 49, 2179–2189, 2004.

Kwiatkowska, E.: Comparisons of daily global ocean color data sets: MODIS-Terra/Aqua and SeaWiFS, NASA Technical Memorandum, Validation, Data Merger and Other Activities Accomplished by SIMBIOS Project: 2002–2003, edited by: Fargion, G. S. and McClain, C. R., chap. 2, NASA-GSFC, 2003.

Kwiatkowska, E. J. and Fargion, G. S.: Application of machine-learning techniques towards the creation of a consistent and calibrated chlorophyll concentration baseline dataset using remotely sensed ocean color data, IEEE T. Geosci. Remote, 41, 2844–2860, 2003.

Longhurst, A. R., Sathyendranath, S., Platt, T., and Caverhill, C.: An estimate of global primary production in the ocean from satellite radiometer data, J. Plank. Res., 17, 1245–1271, 1995.

Longhurst, A. R.: Ecological Geography of the Sea. San Diego, Academic Press, 398 pp., 1998.

Maritorena, S. and Siegel, D. A.: Consistent merging of satellite oceancolor data sets using a bio-optical model, Remote Sens. Environ., 94, 429–440, 2005.

Marrari, M., Hu, C., and Daly, K.: Validation of SeaWiFS chlorophyll *a* concentrations in the Southern Ocean: A revisit, Remote Sens. Environ., 105, 367–375, 2006.

McClain, C. R.: SIMBIOS background, NASA Technical Memorandum, 1999-208645, SIMBIOS Project 1998 Annual Report, chap. 1, 1–3, edited by: McClain, C. R. and Fargion, G. S., NASA-GSFC, 1998.

McClain, C. R., Feldman, G. C., and Hooker, S. B.: An overview of the SeaWiFS project and strategies for producing a climate research quality global ocean bio-optical time series, Deep-Sea Res. II, 51, 5–42, 2004.

Mélin, F., Berthon, J.-F., and Zibordi, G.: Assessment of apparent and inherent optical properties derived from SeaWiFS with field data, Remote Sens. Environ., 97, 540–553, 2005.

Mélin, F. and Zibordi, G.: An optically-based technique for producing merged spectra of water leaving radiances from ocean color remote sensing, Appl. Optics, 46, 3856–3869, 2007.

Mélin, F., Zibordi, G., and Berthon, J.-F.: Assessment of satellite ocean color products at a coastal site, Remote Sens. Environ., 110, 192–215, 2007.

Mélin, F., Zibordi, G., and Djavidnia, S.: Merged series of normalized water leaving radiances obtained from multiple satellite missions for the Mediterranean Sea, Adv. Space Res., 43, 423–437, 2009.

Mélin, F.: Global distribution of the random uncertainty associated with satellite derived Chl *a*, IEEE Geosci. Remote Sens. Lett., 7, 220–224, doi:10.1109/LGRS.2009.2031825, 2010.

Mélin, F., Clerici, M., Zibordi, G., Holben, B. N., and Smirnov, A.: Validation of SeaWiFS and MODIS aerosol products with globally-distributed AERONET data, Remote Sens. Environ., 114, 230–250, doi:10.1016/j.rse.2009.09.003, 2010.

Morel, A. and Maritorena, S.: Bio-optical properties of oceanic waters: A reappraisal, J. Geophys. Res., 106, 7163–7180, 2001.

Morel, A., Antoine, D., and Gentili, B.: Bidirectional reflectance of oceanic waters: accounting for Raman emission and varying particle scattering phase function, Appl. Optics, 41, 6289–6306, 2002.

Morel, A. and Antoine, D.: Pigment index retrieval in Case 1 waters, MERIS Algorithm Theoretical Basis Document 2.9, 25 pp., 2007.

Morel, A., Huot, Y., Gentili, B., Werdell, P. J., Hooker, S. B., and Franz, B. A.: Examining the consistency of products derived from various ocean color sensors in open ocean (Case 1) waters in the perspective of a multi-sensor approach, Remote Sens. Environ., 111, 69–88, 2007.

Murtugudde, R. G., Signorini, S. R., Christian, J. R., Busalacchi, A. J., McClain, C. R., and Picaut, J.: Ocean color variability of the tropical Indo-Pacific basin observed by SeaWiFS during 1997–1998, J. Geophys. Res., 104, 18351–18366, 1999.

Oguz, T., Deshpande, A. G., and Malanotte-Rizzoli, P.: The role of mesoscale processes controlling biological variability in the Black Sea coastal waters: inferences from SeaWiFS-derived surface chlorophyll field, Cont. Shelf Res., 22, 1477–1492, 2002.

Oguz, T. and Ediger, D.: Comparison of in situ and satellite-derived chlorophyll pigment concentrations, and impact of phytoplankton bloom on the suboxic layer structure in the western Black Sea during May–June 2001, Deep-Sea Res. II, 53, 1923–1933, 2006.

O'Reilly, J. E., Maritorena, S., Siegel, D. A., O'Brien, M. C., Toole, D. A., Mitchell, B. G., Kahru, M., Chavez, F. P., Strutton, P., Cota, G. F., Hooker, S. B., McClain, C. R., Carder, K. L., Mueller-Karger, F. E., Harding, L., Magnusson, A., Phinney, D., Moore, G. F., Aiken, J., Arrigo, K. R., Letelier, R., and Culver, M.: Ocean color chlorophyll *a* algorithms for SeaWiFS, OC2, and OC4: Version 4, NASA Technical Memorandum, 2000-206892, vol. 11, Chap. 2, 9–23, edited by: Hooker, S. B. and Firestone, E. R., NASA-GSFC, Greenbelt, Maryland, 2000.

Pottier, C., Garçon, V., Sudre, J., Larnicol, G., Schaeffer, P., and Le Traon, P.-Y.: Merging SeaWiFS and MODIS/Aqua ocean color data in North and equatorial Atlantic using weighted averaging and objective analysis, IEEE T. Geosci. Remote, 44, 3436–3451, 2006.

Quinn, P. K., Coffman, D. J., Bates, T. S., Miller, T. L., Johnson, J. E., Voss, K. J., Welton, E. J., and Neusüss, C.: Dominant aerosol chemical components and their contribution to extinction during the Aerosols99 cruise across the Atlantic, J. Geophys. Res., 106, 20783–20809, 2001.

Ramanathan, V., Crutzen, P. J., Lelieveld, J., Mitra, A. P., Althausen, D., Anderson, J., Andreae, M. O., Cantrell, W., Cass, G. R., Chung, C. E., Clarke, A. D., Coakley, J. A., Collins, W. D., Conant, W. C., Dulac, F., Heintzenberg, J., Heymsfield, A. J., Holben, B. N., Howell, S., Hudson, J., Jayaraman, A., Kiehl, J. T., Krishnamurti, T. N., Lubin, D., McFarquhar, G., Novakov, T., Ogren, J. A., Podgorny, I. A., Prather, K., Priestley, K., Prospero, J. M., Quinn, P. K., Rajeev, K., Rasch, P., Rupert, S., Sadourny, R., Satheesh, S. K., Shaw, G. E., Sheridan, P., and Valero, F. P. J.: Indian Ocean Experiment: an integrated analysis of the climate forcing and effects of the great Indo-Asian haze, J. Geophys. Res., 106, 28371–28398, 2001.

Rast, M., Bezy, J. L., and Bruzzi, S.: The ESA Medium Resolution Imaging Spectrometer MERIS - A review of the instrument and its mission, Int. J. Remote Sens., 20, 1681–1702, 1999.

Salama, M. S. and Stein, A.: Error decomposition and estimation of inherent optical properties, Appl. Optics, 48, 4947–4962, 2009.

Salomonson, V. V., Barnes, W. L., Maymon, P. W., Montgomery, H.E ., and Ostrow, H.: MODIS: Advanced facility instrument for studies of the Earth as a system, IEEE T. Geosci. Remote, 27, 145–152, 1989.

Sancak, S., Besiktepe, S. T., Yilmaz, A., Lee, M., and Frouin, R.: Evaluation of SeaWiFS chlorophyll-a in the Black and Mediterranean Seas, Int. J. Remote Sens., 26, 2045–2060, 2005.

Taylor, K. E.: Summarizing multiple aspects of model performance in a single diagram, J. Geophys. Res., 106, 7183–7192, 2001.

Vantrepotte, V. and Mélin, F.: Temporal variability of 10-year global SeaWiFS time-series of phytoplankton chlorophyll-a concentration, ICES J. Mar. Sci., 66, 1547–1556, 2009.

Vichi, M., Masina, S., and Navarra, A.: A generalized model of pelagic biogeochemistry for the global ocean ecosystem. Part II. Numerical simulations, J. Mar. Syst., 64, 110–134, 2007.

Vinoj, V. and Satheesh, S. K.: Measurements of aerosol optical depth over Arabian Sea during summer monsoon season, Geophys. Res. Lett., 30, 1263, doi:10.1029/2002GL016664, 2003.

Volpe, G., Santoleri, R., Vellucci, V., Ribera d'Acalá, M., Marullo, S., and D'Ortenzio, F.: The colour of the Mediterranean Sea: Global versus regional bio-optical algorithms evaluation and implication for satellite chlorophyll estimates, Remote Sens. Environ., 107, 625–638, 2007.

Wilson, C. and Coles, V. J.: Global climatological relationships between satellite biological and physical observations and upper ocean properties, J. Geophys. Res., 110, C10001, doi:10.1029/2004JC002724, 2005.

Yoder, J. A., McClain, C. R., Feldman, G. C. and Esaias, W. E: Annual cycles of phytoplankton chlorophyll concentrations in the global ocean: A satellite view, Global Biogeochem. Cy., 7, 181–193, 1993.

Zhang, C., Hu, C., Shang, S., Müller-Karger, F., Li, Y., Dai, M., Huang, B., Ning, X., and Hong, H.: Bridging between SeaWiFS and MODIS for continuity of chlorophyll-a concentration assessments off Southeastern China, Remote Sens. Environ., 102, 250–263, 2006.

Zibordi, G., Strömbeck, N., Mélin, F., and Berthon, J.-F.: Tower based radiometric observations at a coastal site in the Baltic Proper, Estuar. Coast. Shelf Sci., 69, 649–654, 2006.

Zibordi, G., Berthon, J.-F, Mélin, F., D'Alimonte, D., and Kaitala, S.: Validation of satellite ocean color primary products at optically complex coastal sites: northern Adriatic, northern Baltic Proper and Gulf of Finland, Remote Sens. Environ., 113, 2574–2591, 2009.